Layerwise monitoring of electron beam melting via backscatter electron detection

Christopher Arnold
Chair of Materials Science and Engineering for Metals, Friedrich-Alexander University Erlangen-Nürnberg, Erlangen, Germany
Christoph Pobel and Fuad Osmanlic
Joint Institute of Advanced Materials and Processes, Friedrich-Alexander University Erlangen-Nürnberg, Fürth, Germany, and
Carolin Körner
Chair of Materials Science and Engineering for Metals, Friedrich-Alexander University Erlangen-Nürnberg, Erlangen, Germany and
Joint Institute of Advanced Materials and Processes, Friedrich-Alexander University Erlangen-Nürnberg, Fürth, Germany

Abstract

Purpose – The purpose of this study is the introduction and validation of a new technique for process monitoring during electron beam melting (EBM).

Design/methodology/approach – In this study, a backscatter electron detector inside the building chamber is used for image acquisition during EBM process. By systematic variation of process parameters, the ability of displaying different topographies, especially pores, is investigated. The results are evaluated in terms of porosity and compared with optical microscopy and X-ray computed tomography.

Findings – The method is capable of detecting major flaws (e.g. pores) and gives information about the quality of the resulting component.

Originality/value – Image acquisition by evaluating backscatter electrons during EBM process is a new approach in process monitoring which avoids disadvantages restricting previously investigated techniques.

Keywords Quality control, Additive manufacturing, Scanning electron microscopy, Electron beam melting, Porosity, Optical microscopy, Process monitoring, Backscatter electrons, X-ray computed tomography

Paper type Research paper

1. Introduction

Electron beam melting (EBM) is a metal additive manufacturing process based on layerwise and selective powder consolidation. Due to its ability to produce complex geometries and to process sophisticated metal alloys, EBM arouses interest in challenging fields like medical and aerospace industry. This goes along with high requirements concerning process control and repeatability which is currently seen as barrier for industrial breakthrough of additive manufacturing technologies (Grasso and Colosimo, 2017). To ensure a high quality of the manufactured components, various process parameters have to be controlled and therefore to be monitored. Lately, a strong reviewing activity (Grasso and Colosimo, 2017; Everton *et al.*, 2016; Mani *et al.*, 2017) demonstrated the continued demand for suitable process monitoring tools in the field of metal additive manufacturing.

EBM is an additive powder-bed fusion process. A rake system within a vacuum chamber is used to apply a defined powder layer. As a first step, the powder layer is slightly sintered by heating it up with a fast and defocused electron beam. The resulting particle connectivity provides sufficient electrical conductivity and mechanical stability for the next step in which a focused electron beam selectively melts the current cross-section of the desired geometry. Afterwards, the next powder layer is applied and the cycle repeated until the final solid part is obtained.

In case of EBM process, most of the work done on process monitoring concentrates on using infrared thermography for image acquisition (Schwerdtfeger *et al.*, 2012; Price *et al.*, 2012; Rodriguez *et al.*, 2012; Dinwiddie *et al.*, 2013). By evaluating the temperature distribution across the layer, information about surface condition may be obtained and correlated with local defects, e.g. pores. Drawback of this method is the susceptibility of light optical systems to metalization due to evaporation from the melt pool (Schwerdtfeger *et al.*, 2012; Dinwiddie *et al.*, 2013). This has to be counteracted by

The current issue and full text archive of this journal is available on Emerald Insight at: **www.emeraldinsight.com/1355-2546.htm**

Rapid Prototyping Journal
24/8 (2018) 1401–1406
Emerald Publishing Limited [ISSN 1355-2546]
[DOI 10.1108/RPJ-02-2018-0034]

The authors gratefully acknowledge funding by the Dobeneck-Technologie-Stiftung and by the Deutsche Forschungsgemeinschaft (DFG) through the Collaborative Research Center SFB 814, Project B2.

Received 2 February 2018
Revised 27 April 2018
18 May 2018
Accepted 26 May 2018

additional protection systems like a mechanical shutter (Schwerdtfeger *et al.*, 2012; Dinwiddie *et al.*, 2013) or a spooling film (Dinwiddie *et al.*, 2013). Furthermore, the size of the beam column prevents a co-axial arrangement of the imaging system (Schwerdtfeger *et al.*, 2012) leading to distortions and hence a varying spatial resolution.

Besides these scientific approaches, there is also a commercial system called Arcam LayerQam™ offered by EBM system developer *Arcam AB (Mölndal, Sweden)*. It works in the range of visible light with some extension into the IR region and therefore suffers the same drawbacks that were mentioned before.

Aim of this work is to introduce an alternative EBM monitoring method which detects backscatter electrons (BSE) and acquires an electron optical (ELO) image in a way comparable to scanning electron microscopy (SEM). BSEs originate from elastic collisions between electrons of the incident beam and substrate atoms. A part of the backscattered electrons hits the BSE detector which is located circular around the beam shortly above the build chamber as depicted in Figure 1. The signal intensity correlates with the number of backscattered electrons which in particular is a function of beam current, atomic number of sample atoms and surface topography. By scanning an area in a defined pattern, an intensity map, i.e. an image, may be obtained. While this basic principle is certainly further elaborated in SEM analysis, the same plane technique is used for some time in electron beam welding (Schiller *et al.*, 1977).

The method was used for layerwise image acquisition and flaw detection during build process. The results were validated against X-ray computed tomography and optical microscopy of the final sample.

2. Experimental

The additive manufacturing process was performed using an in-house development EBM system which combines the vacuum chamber, including powder management and build tank, of an *Arcam EBM S12* and an electron beam welding gun by *pro-beam AG & CO. KGaA (Planegg, Germany)*. The gun operates with an acceleration voltage of 60 kV, while the tungsten filament delivers a beam power up to 6 kW. As an outstanding feature, the system has incorporated the aforementioned BSE detector which provides the possibility of recording ELO images.

The cuboid sample with dimensions of $15 \times 15 \times 22.5\ mm^3$, and its columnar supports were build on a steel base plate with a constant layer thickness of 50 μm. Feedstock was gas-atomized Ti-6Al-4V powder supplied by *Tekna Advanced Materials Inc. (Sherbrooke, Canada)* with a particle size distribution between 45 and 105 μm.

The process parameters for Ti-6Al-4V were chosen according to previous investigations (Jüchter *et al.*, 2014). The preheating was set to operate the process at a target temperature of 1023 K (750°C). Furthermore, a controlled vacuum of 2×10^{-3} mbar of He atmosphere was applied. The cross-section was melted using a standard hatch pattern whereby the scan direction of adjacent hatch lines was alternated by 180°, often referred to as a snake-like or back-and-forth manner. The line spacing during hatching was constant at 100 μm while contour melting was not applied. The hatch direction was rotated by 90° after each layer.

Object of investigation was the consolidation behavior of the bulk material as a function of energy input. At a constant deflection speed of 2 m/s, the hatching beam power was modified every 2.5 mm of build height. The 2.5 mm are equivalent to 50 layers, which is an empirical value to account for transition effects between sections. Starting below process window of dense samples at a value of 120 W the beam power was increased in four equidistant steps to 165, 210, 255 and 300 W where dense layers were produced. Subsequently, the power was accordingly decreased to 120 W again to account for hysteresis effects. The result was a sample of nine stacked sections with different energy input and therefore varying density (Figure 2).

Figure 1 Left: Schematic diagram of an electron beam melting system for metal additive manufacturing

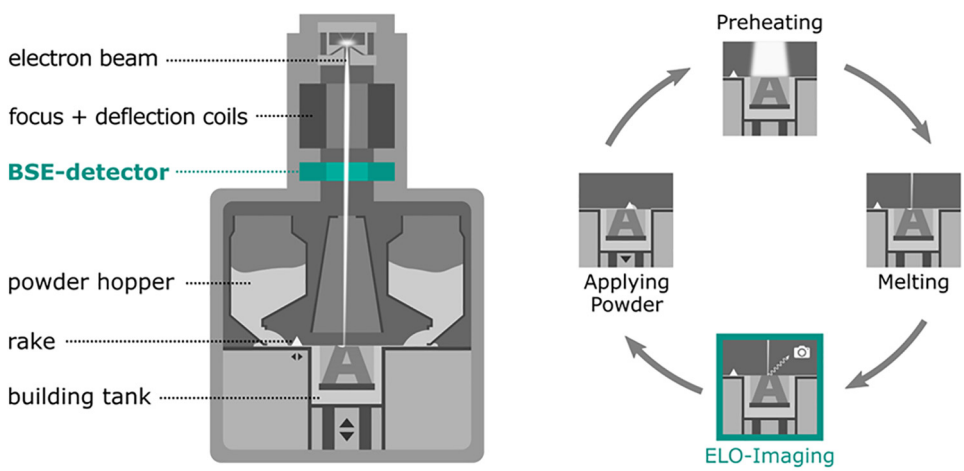

Notes: In the experiment, a detector for BSE was installed shortly above the build chamber and used for ELO image acquisition. Right: Single steps of the EBM cycle. The ELO image acquisition was introduced between the melting step and the application of a new powder layer

Figure 2 Schematic illustration of specimen geometry and variation of beam power

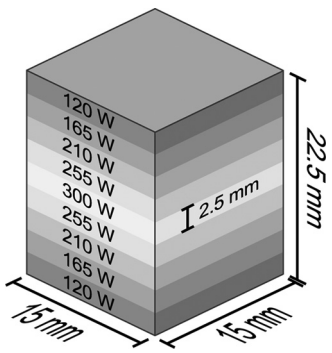

The BSE detector was used during the whole process to capture post-hatching ELO images of the sample surface. The pixel resolution of 60 μm/px was chosen correspondingly to the scale of features that are expected to be detected by using an electron beam with the available diameter of about 300 μm. To receive a suitable backscatter signal, the exposure time was set to 0.1 μs/px and the beam current to 7 mA.

Information about sub-surface structures (e.g. closed pores) is limited by the penetration depth of the electron beam. The estimation by Kanaya and Okayama (using material data for pure titanium and an electron energy of 60 keV) returns a maximum range of approximately 17 μm (Kanaya and Okayama, 1972). Only flaws located between the surface and this maximum range affected the backscatter signal. Taking into account the beam diameter of 300 μm, penetration depth and hence sub-surface information was negligible in the following investigation.

The as-build sample was removed from the base plate and cut longitudinally along the build direction into two pieces. Afterwards, the cross-section was prepared by grinding with water-lubricated SiC paper, mechanical polishing with 3 μm diamond suspension and a final chemical polishing step (50 mL *Struers OP-S NonDry*, 50 mL dist. H_2O, 10 g KOH, 10 mL H_2O_2). The prepared microsection was investigated by optical microscopy (OM) using a Leica DM6000 M. The precise image stitching mode of the microscope was used to create a high resolution image (13 μm/px) of the entire cross-section to be further evaluated in terms of porosity.

As an alternative approach to quantify porosity one half of the as-build sample was analyzed by X-ray computed tomography (CT). The CT-system by *Fraunhofer Institute EZRT* used an acceleration voltage of 150 kV to create transverse slices of the sample with a voxel size of 26 μm.

To simplify a qualitative visual comparison between the three imaging methods, a virtual longitudinal cross-section of the sample was calculated from the layerwise captured ELO-images. Taking into account the ratio between pixel-size and layer thickness, the ELO-images were stacked upon each other in chronological order to reconstruct a 3D density map of the sample. The latter was afterwards virtually cut in longitudinal direction.

A common feature of the three imaging methods is the effectiveness of pores as intensity sink for the corresponding measuring signal. The intensity I is correlated to the pixel values of the captured grayscale images, i.e. low values representing low intensity. To a certain extent, dark areas can therefore be assumed as porous, in contrast to brighter ones which are supposed to be denser.

A scalar quantity representing porosity was determined by calculating the normalized mean grayscale value $\overline{I}$ for each imaging method as a function of build height z [equation (1)]. It had to be considered, that the imaging methods transform real space (x, y, z) into discrete space (i, j, k), while n is the total number of pixels in k-direction. ELO- and CT-image averaging was performed based on the transverse 2D-slices obtained from image acquisition and image reconstruction, respectively. The OM-image was analyzed by calculating the mean grayscale value for each row of the stitched bitmap image (j = *const.*). All values were normalized using the respective maximum within each method to the interval [0, 1] to account for different color depths. Correlation with build height was achieved by using corresponding image resolution R_z (in px/m):

$$\overline{I}(z) = \frac{\sum_{i,j} I_{i,j,k}}{\max\left(\sum_{i,j} I_{i,j,0}, \ldots, \sum_{i,j} I_{i,j,n}\right)} \text{ with } k = \text{int}(R_z \cdot z) \quad (1)$$

3. Results

Figure 3 shows exemplary transverse sections of the cuboid sample for all power levels. The images were obtained by in-process layer-wise ELO image acquisition and post-process X-ray computed tomography. It can be stated for both imaging methods that the number of defects decreases with increasing beam power.

The decline in porosity can be explained by the amount of energy available for powder consolidation. Considering other process parameters like deflection speed and hatch line spacing, 120 W is far below the process window of the dense samples. With increasing beam power, more energy is available for

Figure 3 Comparison between ELO images recorded during process and X-ray computed tomography of the as-build sample (transverse cross-section)

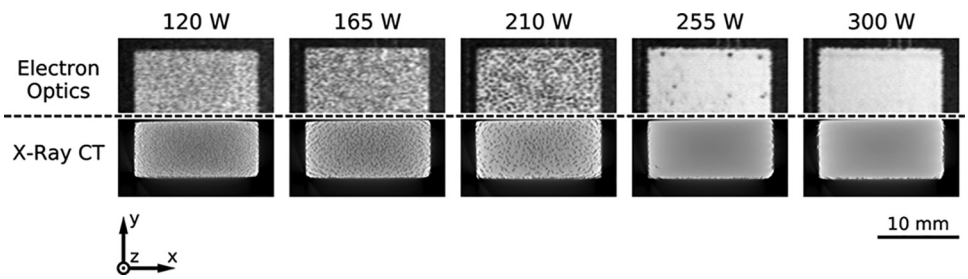

fusing powder and underlying layers, resulting in a smoother surface of the most recent molten layer (Jüchter *et al.*, 2014).

First, it becomes evident that ELO-imaging is capable of visualizing the changing surface topography from a strongly porous to a fully dense structure. The low intensity of a defect can be explained by the angles between the surface normal, the incident beam and the direction to the electron detector. Due to the co-axial position of the detector, the direction of the incident beam and the direction to the electron detector are almost identical. Therefore, increasing the angle between surface normal and the incident beam reduces the number of electrons which are measured by the detector. Additionally, the electrons may be scattered multiple times inside the defect cavity which decreases the signal intensity furthermore.

By taking into account corresponding CT-images, it is assumed that ELO-imaging not only provides information about surface topography but also indicates sites of preferred pore generation and therefore can be used as an estimation for porosity inside the final sample. However, porosity characteristics, i.e. number and size of pores, are not identical.

By stacking the ELO-images layerwise upon each other, a virtual 3D-model of the sample was obtained. Figure 4 includes the virtual centric cross-section through that model in longitudinal direction. To demonstrate the dependency between structure and energy input, the applied power stages are highlighted. It could be seen that a rather small power increase or decrease of 45 W resulted in a distinct modification of the bulk structure. With these transformations happening rather abrupt, it could be stated that porosity was bound very strongly to energy input, and transition regions were limited to height of only a few powder layers.

By comparing upper and lower 255 W section, it was noted that the lower section contained some channel-like porosities while the upper one was quite homogeneous. Bauereiß *et al.* give an detailed explanation of the underlying defect generation mechanism of channel-like porosity (Bauereiß *et al.*, 2014). The current observation indicates an additional hysteresis effect when varying porosity by changing beam power. Building dense layers on a porous surface would require a higher energy input than building the same layers on a dense surface.

To evaluate the ability of *in situ* ELO-imaging to compete with common post-build analyzing tools, transverse cross-sections obtained by OM and CT are depicted in Figure 4 as well. A visual comparison shows that there is a good qualitative agreement between the three imaging methods. Going into detail by comparing ELO- with CT-image, even certain defects, e.g. the distinctive channel-like porosity in the lower 255 W-section, can be predicted precisely. This distinctive porosity cannot be observed in the OM-image. This is caused by the preparation procedure which impedes getting the same cross-section as in ELO- and CT-imaging.

To quantify particular characteristics and the relationship between the three imaging methods, normalized mean intensities as a function of build height were calculated from respective grayscale images. The charts in Figure 5 show that all imaging methods are capable of displaying the step-wise change in intensity as a function of build height and accordingly beam power. The smoothness of the charts depends on the imaging method and its respective evaluation. X-ray computed tomography delivers a rather smooth curve, while evaluation of the two-dimensional microsection via optical microscopy shows strong variations in the averaged intensity signal. This can be explained with the different sample sizes forming the respective average. In this respect, the curve of ELO-imaging lies somewhere in between.

Despite of normalizing the values, there is yet a significant difference between corresponding intensity levels. In case of OM-and CT-imaging, this can be solely explained by different

Figure 4 Comparison of longitudinal cross-sections obtained by three different imaging methods

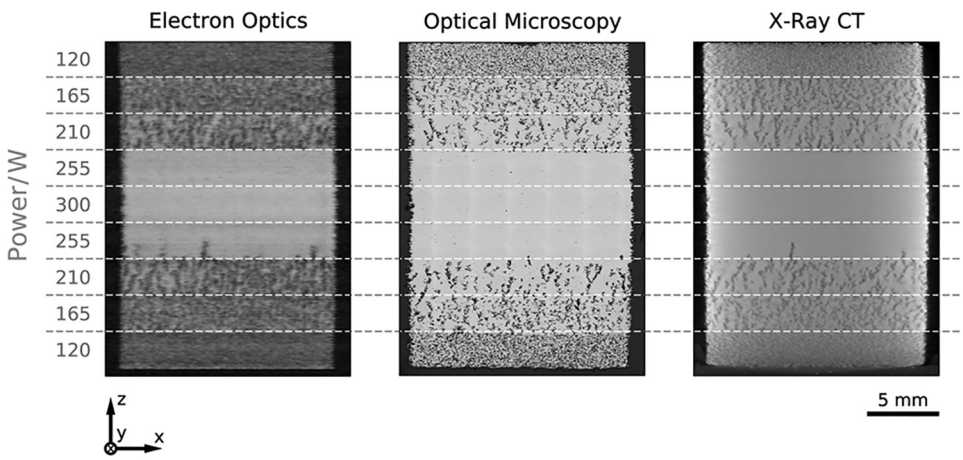

Notes: In the case of electron optics (ELO), the layer images were stacked in chronological order to create a three-dimensional object which was afterwards virtually cut in longitudinal direction. Optical microscopy (OM) was performed on a prepared microsection, while X-ray computed tomography (CT) used an as-build half of the cuboid sample. With ELO-image and CT-image showing identical cross-sections of the sample, this was not possible for OM due to the preparation procedure

Figure 5 Quantitative evaluation of porosity by plotting the normalized mean intensity returned by the three imaging methods as a function of specimen height

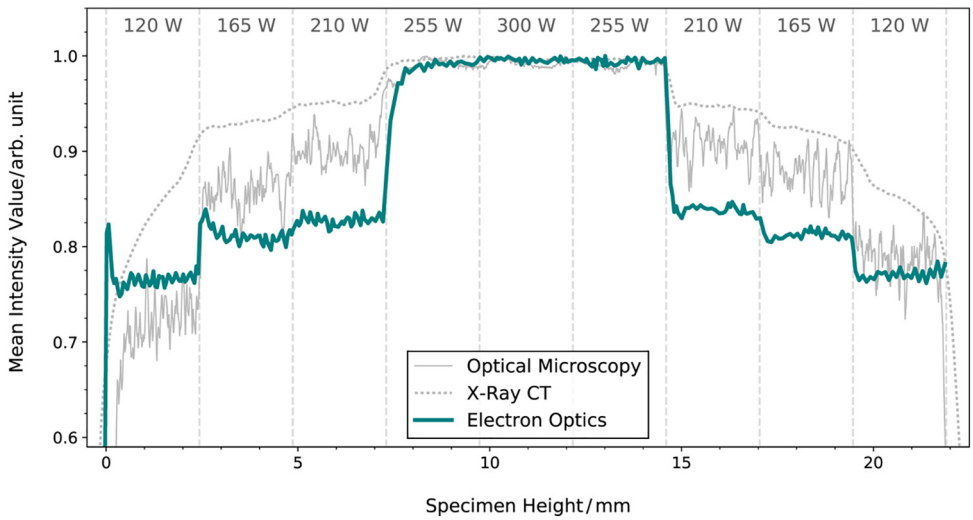

resolutions and contrasts provided by the respective measuring signal. Furthermore, ELO-images are restricted to surface topography which introduces an additional source of variation. The step height of mean intensity at 210/255 W-transitions, i.e. in the region of critical energy input for material consolidation, is exceptionally high for ELO-imaging. It appears that critical energy input has a higher influence on surface topography than on porosity of the final bulk material. Therefore it can be concluded that ELO-imaging overestimates the the resulting porosity, a fact that can also be qualitatively deduced from Figure 4.

When comparing 210/255 W and 255/210 W-transition, the curve slopes of all three methods seem to be slightly steeper for power decrease. This can be seen as an additional indication of the aforementioned hysteresis effect.

4. Discussion

In comparison with optical microscopy and X-ray computed tomography, ELO imaging via BSEs is characterized by some outstanding features, while there are also some restrictions to be considered.

First, the spatial resolution is currently quite low with respect to OM- and CT-imaging. Therefore the amount of possible flaws to be detected via ELO-imaging is limited to major defects. In addition, ELO-imaging is restricted to recording layer surfaces and reconstructing a three-dimensional model afterwards. It was demonstrated that some discrepancies result from this approach, especially the overestimation of porosity by ELO-imaging. Presumably, a relevant amount of defects that are present on the surface and therefore on ELO-image is partially filled and even closed during melting of subsequent layers. As a result, the absolute number of pores and their size is smaller in the as-build part. The suitability of ELO-imaging as a tool for quality control is yet not restricted because flaws are reliably detected, in worst-case overestimated.

As can be seen in the lower 255 W-section in Figure 4, OM-imaging of a 2D-cross-section is not capable of giving full information about porosity. If the defect density is low enough that no defect is cut by the cross-section, the quality of the sample might be overrated. Analysis via X-ray CT delivers full 3D-information but has to consider other restrictions, e.g. concerning specimen size. In contrast, ELO-imaging is capable of reconstructing 3D-information about major defects without additional requirements to be considered.

Furthermore, ELO-imaging offers some unique features which make it an outstanding tool for EBM process observation. In contrast to OM and CT, ELO-imaging is an in-process method which allows generation of information about the current layer in real-time. It not only does enable the operator to manually adjust parameters during process but also inheres the possibility to connect the evaluation to closed-loop control for advanced processing strategies and faster process window determination.

Thermography as an alternative in-process monitoring tool is either restricted to small fields of view of some square millimeters (Price *et al.*, 2012) or spatial resolutions above 100 μm/px (Schwerdtfeger *et al.*, 2012; Rodriguez *et al.*, 2012), depending on the lenses in use. ELO-imaging is capable of recording the entire build area with a resolution below 100 μm/px.

Unlike other methods, the BSE detector is robust in terms of process temperature, X-radiation and powder contamination. Moreover, metalization of the BSE-detector does not decrease the quality of the measured signal over time as seen in optical methods (Schwerdtfeger *et al.*, 2012; Dinwiddie *et al.*, 2013). Particular protection of the detector like shutters and windows may therefore be omitted. This enables the integration of the detector inside the building chamber in a co-axial position which is a novelty for the EBM process. The reduced optical aberration resulting from a co-axial sensor position improves image quality furthermore.

The BSE detector not only does improve in-process quality control but also simplifies the evaluation of beam quality in advance. By comparing a defined object and its corresponding ELO-image, information about beam-spot shape and size may be obtained and used for documentation and optimization, assuring a steady and high beam quality over a long period.

5. Conclusions

It was shown that image acquisition during EBM process by using BSEs is a promising approach. The spatial resolution is sufficient for detecting major flaws like surface defects while disadvantages restricting other monitoring techniques can be avoided. It was demonstrated that conclusions about the porosity of the final component may be drawn. Therefore, detection of BSEs is already capable of improving the EBM process. The system may be further enhanced, e.g. by introducing additional off-axial detectors to gather more information about surface topography or even calculating a three-dimensional reconstruction of the entire surface topology (Paluszyński and Slówko, 2009). Such a tool would open up new possibilities for process understanding and control. By reducing electron beam-spot size, a higher spatial resolution can be expected. The beam-spot size results from filament type, focus lenses and beam current. One future objective to pursue would be the determination of an optimal trade-off between requirements of EBM process and ELO-imaging.

In the field of EBM technology, the investigated approach is a first step in combining the powder-bed fusion process with electron beam-based analyzing techniques like electron imaging, electron backscatter diffraction or X-ray spectroscopy. These methods are supposed to deliver advanced information about the process and hence make a big contribution to its further development.

References

Bauereiß, A., Scharowsky, T. and Körner, C. (2014), "Defect generation and propagation mechanism during additive manufacturing by selective beam melting", *Journal of Materials Processing Technology*, Vol. 214 No. 11, pp. 2497-2504.

Dinwiddie, R.B., Dehoff, R.R., Lloyd, P.D., Lowe, L.E. and Ulrich, J.B. (2013), "Thermographic in-situ process monitoring of the electron-beam melting technology used in additive manufacturing", in Stockton, G.R. and Colbert, F.P. (Eds), *Proceedings SPIE 8705, Thermosense: Thermal Infrared Applications XXXV*, 87050K.

Everton, S.K., Hirsch, M., Stravroulakis, P., Leach, R.K. and Clare, A.T. (2016), "Review of in-situ process monitoring and in-situ metrology for metal additive manufacturing", *Materials & Design*, Vol. 95, pp. 431-445.

Grasso, M. and Colosimo, B.M. (2017), "Process defects and in situ monitoring methods in metal powder bed fusion: a review", *Measurement Science and Technology*, Vol. 28 No. 4, p. 044005.

Jüchter, V., Scharowsky, T., Singer, R.F. and Körner, C. (2014), "Processing window and evaporation phenomena for Ti-6Al-4V produced by selective electron beam melting", *Acta Materialia*, Vol. 76, pp. 252-258.

Kanaya, K. and Okayama, S. (1972), "Penetration and energy-loss theory of electrons in solid targets", *Journal of Physics D: Applied Physics*, Vol. 5 No. 1, p. 308.

Mani, M., Lane, B.M., Donmez, M.A., Feng, S.C. and Moylan, S.P. (2017), "A review on measurement science needs for real-time control of additive manufacturing metal powder bed fusion processes", *International Journal of Production Research*, Vol. 55 No. 5, pp. 1400-1418.

Paluszyński, J. and Slówko, W. (2009), "Measurements of the surface microroughness with the scanning electron microscope", *Journal of Microscopy*, Vol. 233 No. 1, pp. 10-17.

Price, S., Cooper, K. and Chou, K. (2012), "Evaluations of temperature measurements by near-infrared thermography in powder-based electron-beam additive manufacturing", *Proceedings of the Solid Freeform Fabrication Symp, University of TX, Austin, TX*, pp. 761-773.

Rodriguez, E., Medina, F., Espalin, D., Terrazas, C., Muse, D., Henry, C., MacDonald, E. and Wicker, R.B. (2012), "Integration of a thermal imaging feedback control system in electron beam melting", *23rd Annual International Solid Freeform Fabrication Symposium-An Additive Manufacturing Conference*, Figure 1, pp. 945-961.

Schiller, S., Panzer, S. and von Ardenne, T. (1977), "Prozeßkontrolle durch Rückstreuelektronen", *ZIS-Mitteilungen*, Vol. 19 No. 2, pp. 238-248.

Schwerdtfeger, J., Singer, R.F. and Körner, C. (2012), "In situ flaw detection by IR-imaging during electron beam melting", *Rapid Prototyping Journal*, Vol. 18 No. 4, pp. 259-263.

Corresponding author

Christopher Arnold can be contacted at: christopher.arnold@fau.de